

# Hydrogen Generation by Means of Hydrolysis Using Activated Al-In-Bi-Sn Composites for Electrochemical Energy Applications

*S.P. du Preez and D.G. Bessarabov\**

HySA Centre of Competence, North-West University (NWU), Potchefstroom Campus, Private Bag X6001, Potchefstroom, 2520, South Africa

\*E-mail: [dmitri.Bessarabov@nwu.ac.za](mailto:dmitri.Bessarabov@nwu.ac.za)

*Received:* 12 April 2017 / *Accepted:* 30 June 2017 / *Published:* 13 August 2017

---

Effective activation compounds are developed to produce hydrogen via hydrolysis of ball-milled Al-In-Bi-Sn composites in tap water at room temperature. Al-In-Bi-Sn composites are successfully activated by 3 h of milling. These composites exhibit hydrogen yields > 85% between 2.5 min (fastest reaction time) and 14 min (slowest reaction time). The intermetallic phases responsible for Al activation, InSn<sub>4</sub>, InBi and In<sub>3</sub>Sn, are selectively synthesized, identified and characterized. The reaction kinetics of each intermetallic phase are determined after ternary composite preparation, i.e., milling Al with In and Bi or Sn. Quaternary composites are also prepared to determine the formation kinetics of the intermetallic phases. These quaternary composites have high hydrogen yields (> 90%) and the reactions are complete within 170 s. The formation of intermetallic phases is responsible for the structural failure of Al, resulting in the size reduction of Al particles. The following are also investigated and quantified: the effects of water volume and reaction temperature on hydrolysis kinetics, and the activation energies of ternary Al composites.

---

**Keywords:** Activated aluminum; Hydrogen generation; Mechanochemical activation

## 1. INTRODUCTION

Hydrogen is a nonpolluting, clean and renewable energy carrier [1]. It has been identified as the most promising future alternative to traditional fossil fuels [2,3] due to its high calorific values [4], abundance and renewability [5]. The majority of hydrogen gas is produced from hydrocarbon sources [6], which produce large quantities of CO<sub>2</sub> gas as a by-product [7]. In addition, traces of CO may be present in hydrogen produced from hydrocarbons and may deteriorate proton exchange membrane fuel cells (PEMFCs) used to convert hydrogen's chemical energy to electrical energy [8]. Hydrogen can be

generated from various hydrocarbon sources, such as biogas [9], natural gas [4], and petroleum [10], whereas non-hydrocarbon hydrogen generation methods includes water electrolysis [9,11], water photo-catalysis [12], metal hydrolysis [11,13], and metal hydride hydrolysis [14]. Combining hydrogen with fuel cells to devices that are able to transform chemical energy into electricity and heat has yet to reach wide-scale application due to certain limitations, e.g., low efficiency, and high costs of hydrogen storage and transport [15]. For example, hydrogen has a low gaseous density of  $0.089 \text{ kg m}^{-3}$ , making the storage (and transport) of hydrogen gas a major limiting factor to the application thereof [4,16]. Ideally, hydrogen should be generated as it is required and consumed as soon as possible after being generated, removing the need for long term storage.

In recent years, research has focused on hydrogen generation by the reaction between a hydrogen source and a metal as hydrolyzing material [17-19]. Water is the most promising candidate as a hydrogen source [20] because it has a high hydrogen content of  $111 \text{ kg m}^{-3}$ , whereas gasoline and pure liquid  $\text{H}_2$  have hydrogen contents of 84 and  $71 \text{ kg m}^{-3}$ , respectively [4,21]. Group IIA and IIIA light metals hold promise as hydrolyzing materials [22]. One such a promising and sustainable metal is aluminum (Al), the most abundant crustal metal on earth [4,23,24]. Al is a lightweight metal with a low density of  $2700 \text{ kg m}^{-3}$  and it can be fully recycled after hydrolysis through the Hall-Héroult process [25]. Furthermore, solid Al is much easier and safer to store than chemical hydrides and other hydrogen carriers [26].

Thus, hydrogen generation via hydrolysis of Al composites has attracted much interest from the scientific community because of the relative simplicity of the system and the high hydrogen storage capacity [27]. The reaction related to hydrogen generation is expressed as follows [5,25,26,28]:



or



The by-products produced in Reactions (1) and (2) are eco-friendly and they have many industrial applications, e.g., in alumina production [26], water treatment, paper making and fire retardation [25].

A major problem during Al hydrolysis, however, is the formation of a thin coherent oxide layer on the surface of Al and its composites, preventing further oxidation and corrosion of the Al [29]. Many methods have been proposed to remove and/or disrupt the oxide layer in efforts to increase the Al reactivity. One such method is the immersion of Al in an alkaline NaOH and/or KOH environment, which causes corrosion of the oxide layer and exposure of fresh Al to water [30-33]. However, due to the corrosive conditions, alternate methods were developed. One such a method is the amalgamation of the surface of Al with Hg, Hg-Zn amalgam [34] or eutectic Ga-In [22,35]. A less expensive and nontoxic method for removing the passive film includes the mechanical milling of Al with water soluble inorganic salts [36,37], carbon [38], metal oxides [39,40], iron [41] or lithium [42]. However, some of these methods have limitations, e.g., manufacturing processes are time consuming, the addition of large quantities (high wt%) of activation compounds is required, and initial and/or overall hydrogen generation rates are low.

Alloying Al with low melting point metals, e.g., Ga, In, Zn, Sn and Bi, has been found to be successful in activating Al for hydrogen generation under mild conditions [4,13,22,36,43]. During Al

composite preparation, melting methods require more energy than mechanochemical methods, hence increasing the cost of such composites. Furthermore, the inclusion of expensive activation compounds (Ga and In) reduces the economic feasibility of the large scale application. To the best of our knowledge, very limited literature is available in the public peer-reviewed domain on the successful mechanochemical activation of Al by means of low melting point metals (excluding Ga) for hydrogen generation purposes. Wang et al. (2013) achieved hydrogen conversion efficiency of close to 100% using a mechanochemically activated Al-Ga-In-Sn 89-3-3-5 wt% composite. The intermetallic phases  $\text{In}_3\text{Sn}$  and  $\text{InSn}_4$  were observed during mechanochemical preparation of the Al-Ga-In-Sn composite. They are suspected to be the major compounds contributing to the activation of Al [44]. A recent study by du Preez and Bessarabov (2017) prepared high hydrogen yielding Al-Bi-In composites by a mechanochemical activation method dissimilar to the one applied in this study [45].

In this study, we attempted to activate Al by a mechanochemical activation method using Bi, In and/or Sn. Activation of Al was successfully achieved using only Bi-In and In-Sn.  $\text{InBi}$ ,  $\text{In}_3\text{Sn}$  and  $\text{InSn}_4$  were selectively synthesized and the reaction kinetics for each of the composites containing intermetallic phases, i.e., Al-BiIn, Al- $\text{In}_3\text{Sn}$  and Al- $\text{InSn}_4$ , were investigated. X-ray diffraction (XRD) was used to confirm the presence of *in-situ* formed intermetallic phases. Formation and reactivity of quaternary Al-In-Bi-Sn was also investigated. The activation metals (Bi, In and Sn) were found to be present on the surface of Al particles, indicating complete consumption of the as-received In, Bi and Sn during the mechanochemical activation process.

## 2. MATERIALS AND METHODS

### 2.1. Materials

The following starting materials were supplied by Sigma-Aldrich (South Africa): Al powder (< 200  $\mu\text{m}$ , 99.5% purity), In shots (+5–2 mm, > 99.9% purity), Bi granules (> 99.99% purity) and Sn powder (< 150  $\mu\text{m}$ , 99.5% purity). Hydrolysis reactions were performed using tap water. Pure nitrogen (99.99%) (Afrox, South Africa) was used during all purging steps.

### 2.2. Aluminum composite compositions and their mechanochemical preparation

Various Al composites with different compositions were prepared. Different amounts of Bi, In and Sn were added to a constant amount of Al (86.91 wt%). The amounts of the respective activation compounds varied between 0 and 10.55 wt%. The total amount of the activation compound was kept at 13.09 wt%. The compositions of ball-milled Al composites are given in Table 1.

Ball milling of Al composite powders was performed in a Retsch PM100 planetary ball mill (Retsch, Germany) under a nitrogen atmosphere. The as-received metals (Al, Bi, In and Sn) were weighed and placed in a 250 mL stainless steel grinding pot with 5 mm stainless steel grinding balls. The grinding ball to powder mass ratio was 30:1. For all composite preparations, the as-received metals were milled for 3 h at 450 rpm.

**Table 1.** Al composite compositions (wt%).

Composite	Compound (wt%)			
	Al	Bi	In	Sn
Al-InSn <sub>4</sub>	86.91	0	2.54	10.55
Al-InBi	86.91	8.38	4.71	0
Al-In <sub>3</sub> Sn	86.91	0	9.82	3.27
A	86.91	3.93	3.93	5.24
B	86.91	6.54	3.93	2.62
C	86.91	3.93	6.54	2.62
D	86.91	3.93	2.62	6.54

After each milling procedure, the ball-milled samples (still in the sealed grinding pots) were allowed to cool to room temperature. To avoid unwanted atmospheric oxidation, hydrolysis experiments with the cooled ball-milled samples were carried out as soon as possible. Composites were stored in an airtight container until required for use. Each composite was ball milled in duplicate. Only composites that displayed a repeatable trend in terms of physical change and size reduction after 3 h of ball milling were investigated, in triplicate. The particles of some Al composites agglomerated to form large particles with low reactivity. These were excluded from this study.

### 2.3. Hydrolysis set-up and hydrogen measurements

Hydrolysis reactions were carried out at standard temperature and pressure in a 100 mL flask reactor with two openings, one for hydrolysis solution addition (by means of a pressure equalizing addition funnel) and the other for hydrogen to escape. The generated hydrogen passed through a gas drier containing a combination of Drierite™ (CaSO<sub>4</sub>) and SiO<sub>2</sub> to remove water vapor prior to hydrogen measurements. The hydrogen volume was measured using the water trap method, as described by Zhao et al. [46]. Hydrogen measurements were performed using 0.2 g composite and 10 mL of reaction solution, unless specified otherwise. The reaction mixtures were left unagitated during all hydrolysis reactions.

### 2.4. Expression of hydrogen generation

Hydrogen production is expressed as conversion yield (%), defined as the volume of hydrogen produced over the theoretical value of hydrogen that should be released assuming that the entire Al content is hydrolyzed. Applying the ideal gas law, approximately 1360 mL per gram of Al can be achieved under standard atmosphere and temperature conditions. The hydrogen generation rate is defined as the amount of hydrogen produced per minute and is expressed as mL min<sup>-1</sup>, with mL referring to the volume of hydrogen generated from 0.2 g Al composite. All hydrolysis reactions had repeatable hydrogen generation values. The data are presented in triplicate. Error bars are not included for ternary composites as the error spread for all hydrolysis reactions was < 3%.

### 2.5. Sample characterization by XRD and SEM

XRD was performed using a Röntgen diffraction system (PW3040/60 X'Pert Pro). A back-loading preparation method was used to determine the crystalline phases present in the Al composites and hydrolysis residues. The samples were scanned using X-rays generated by a copper (Cu)  $K\alpha$  X-ray tube. Measurements were carried out between variable divergence slits and fixed receiving slits. The phases were identified using X'Pert HighScore Plus software (PANalytical).

Surface analysis of the as-received Al powder and ball-milled Al powders was performed using scanning electron microscopy (SEM). A FEI Quanta 200 scanning electron microscope with an integrated Oxford Instruments INCA 200 energy dispersive X-ray spectroscopy (EDS) microanalysis system was used. SEM micrographs were obtained (at various magnifications) to characterize the physical attributes of the investigated materials. Magnification ( $\mu\text{m}$  scale) is indicated on all micrographs presented (Figs 1–3). SEM-EDS were used to confirm the distribution of activation compounds on the surface of Al particles.

## 3. RESULTS AND DISCUSSION

### 3.1. Effects of ball milling on characteristics of Al composite particles

Repetitive plastic deformation of metals generally changes their microstructure, affects the magnitude of residual stresses and redistributes the constituents [47]. Initially, the Al composites described in this paper were milled for various periods of time and then contacted with water to determine an optimal milling time. Al composites milled for < 3 h (0.5, 1 and 2 h) had hydrogen yields of 5–35%. Visually, it was clear that the fine powders of the as-received Al powder and the activation compounds coagulated during the first 2 h of ball milling to form large flake-like particles. It was accepted that initial ball milling of fine Al powder with In, Bi and/or Sn caused particles to undergo cold welding, which increased the particle size of the powders dramatically. Some reactivity was observed, which is indicative of initial Al composite activation, but it was considered to be insignificant.

After 3 h of milling, particles changed from a flake-like morphology to a fine powder, coupled with a large increase in reactivity. Although it is unclear what causes this key change in morphology, this phenomenon can be explained on the basis of two mechanisms. (1) Ductile and malleable particles will agglomerate due to cold welding as a result of Al composite particles caught between milling ball impacts, i.e., ball–ball and ball–milling chamber, and undergo elastic deformation, until a certain stress-to-strain point is reached. (2) The Al particles then become deformed during the milling process, consequently increasing the hardness of these particles due to work hardening. The work hardened particles will then plastically deform and fracture, resulting in a decrease in particle size [48,49]. A similar trend was observed by Razavi-Tousi and Szpunar [50]; high energy ball-milled Al powder particles cold welded together, followed by a sudden decrease in particle size after a certain period of

ball milling. The fine Al composite powders produced by ball milling indicated that the as-received materials were milled into a homogenous powder with regard to particle size and distribution.

Fig. 1a shows a SEM image of the as-received Al powder and Fig. 1b an image of a 3 h ball-milled Al-9.82 wt% In-3.27 wt% Sn mixture before hydrolysis. The shape of the as-received Al powder changed from the initial 100–300  $\mu\text{m}$  strand-like morphology to platelet morphology 7–70  $\mu\text{m}$  in size. Fig. 1b shows that small fractured particles of the composite are embedded onto larger particles, leading to an increase in the deformities and defects of both types of particles, i.e., the smaller fractured and larger welded particles.

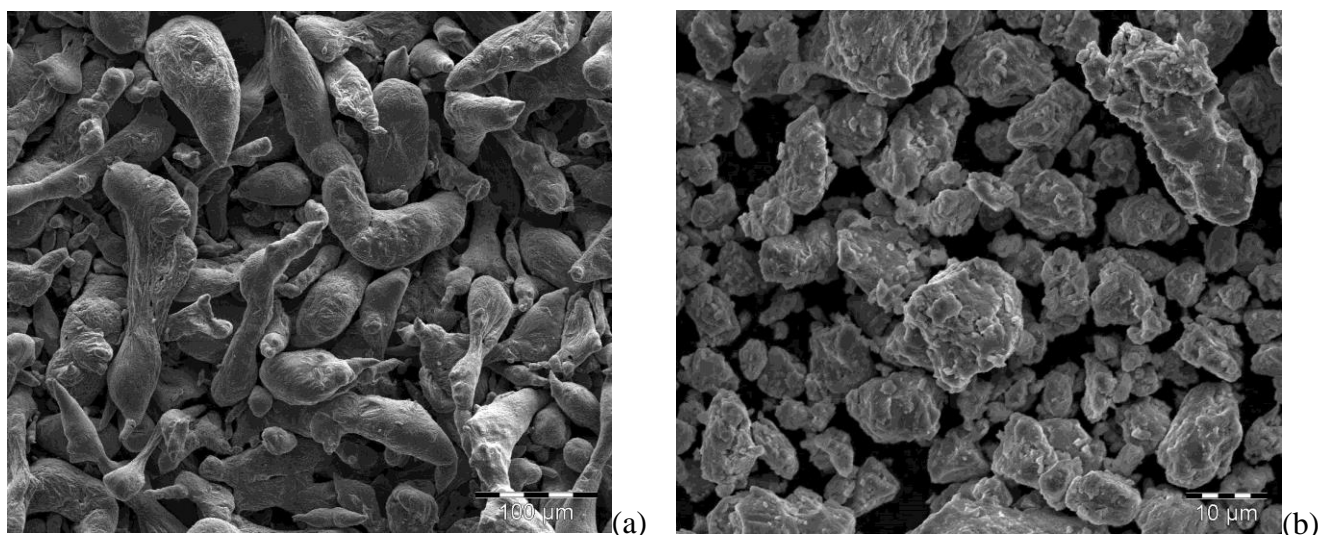


**Figure 1.** SEM micrographs of (a) as-received Al powder and (b) 3 h milled Al-9.82 wt% In-3.27 wt% Sn mixture.

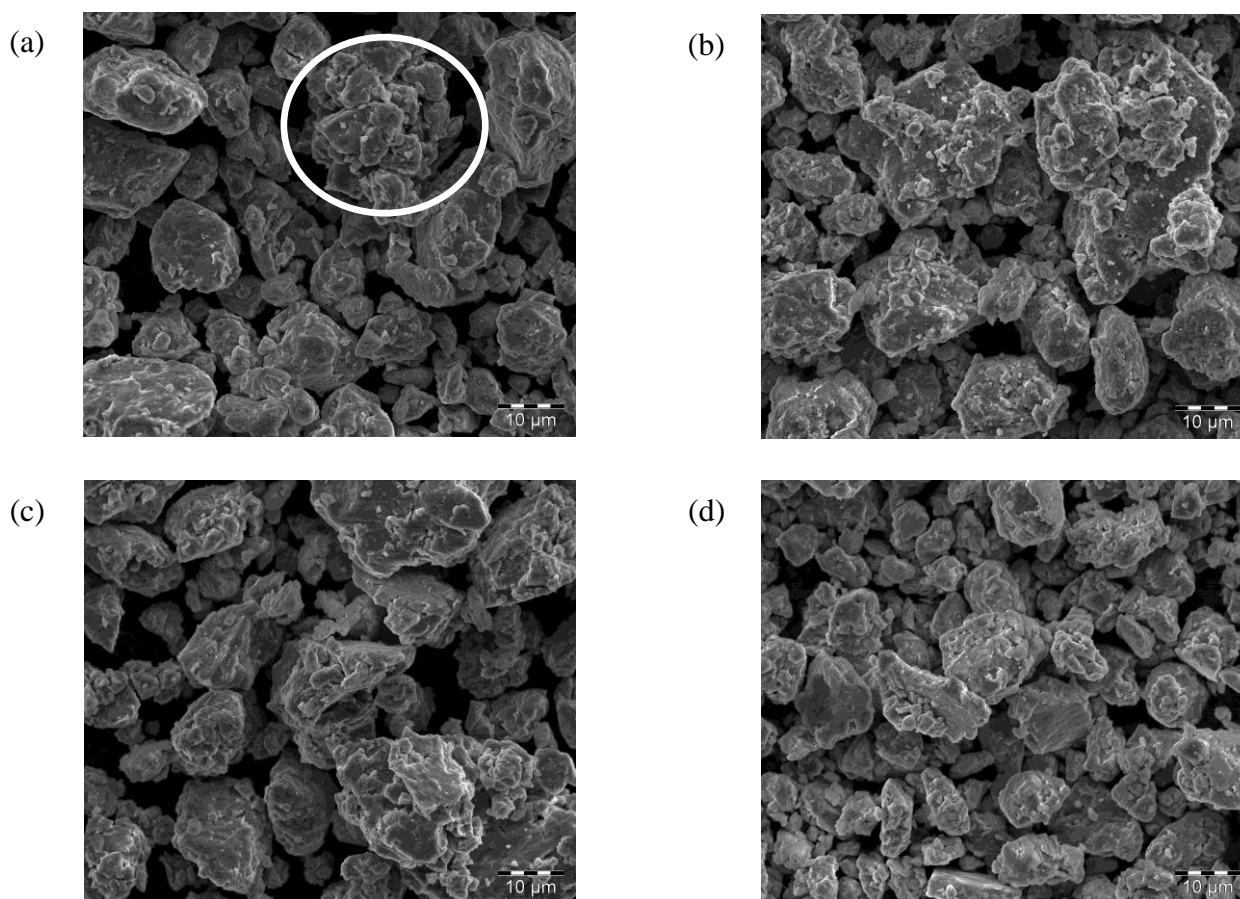
After a certain period of ball milling, steady state equilibrium was reached between the rate of cold welding and the rate of fracturing; cold welding increases the average particle size and fracturing decreases it. Smaller particles are able to resist deformation without fracturing and they tend to weld onto larger particles, with an overall tendency to drive both very fine and very large particles towards an intermediate size [49,51]. A relatively large change in particle size, accompanied by the presence of both small and large particles, is shown in Fig. 1b. It indicates the presence of steady state equilibrium between the rate of welding and fracturing.

Fig. 2 shows various SEM micrographs illustrating ball-milled Al-In-Sn/Bi composite particles and quaternary Al Composite A (Al-3.93 wt% Bi-3.93 wt% In- 5.24 wt% Sn). The clustered particle encircled in Fig. 2a clearly indicates cold welding of smaller Al particles onto each other, forming a larger clustered particle. These clustered particles contain numerous deformities and irregularities, enabling water to freely penetrate deep within the particle. The majority of particles consist of larger solid particles, with smaller particles embedded on their surfaces. The reaction surface of clustered particles presented in Fig. 2 facilitates a larger surface area than single, smoother particles. This is due to the presence of previously mentioned deformities and irregularities. A larger reaction surface

implies a greater particle surface:water contact boundary, which will expedite the Al hydrolysis reaction. All of the reported composites prepared in this study had similar morphologies to the composites presented in Fig. 2 (confirmed by SEM), but these micrographs were not included in this paper.

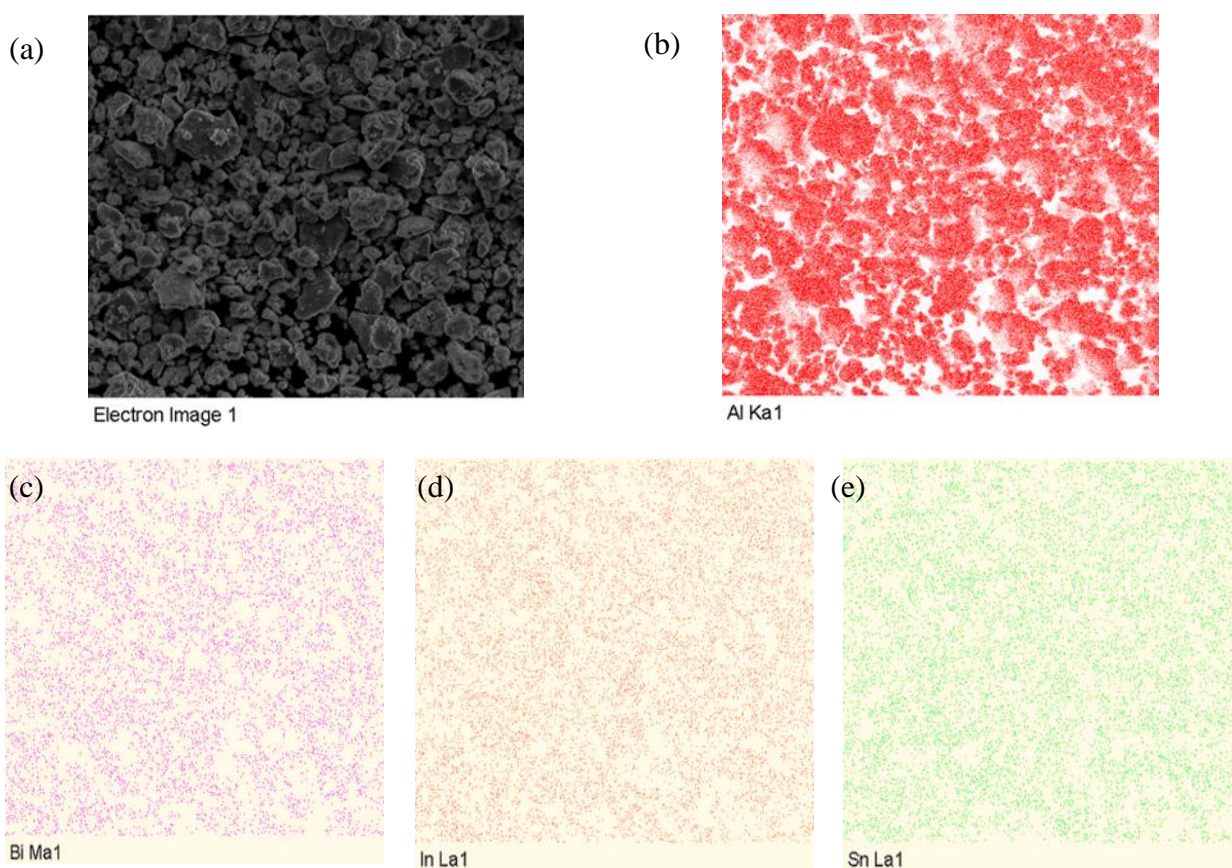
It is evident from Figs 1 and 2 that the particle size of the as-received Al powder was successfully reduced. However, for the Al particles to act as hydrolyzing materials under ambient conditions, the reduction of particle size alone will not suffice. As previously mentioned, the formation of a thin coherent oxide layer on the surface of the Al particles has to be disrupted, exposing the underlying fresh Al to water. Thus, successful activation of Al particles depends on the distribution of the activation compounds (Bi, In and Sn) over the entire surface of the Al particles.

Fig. 3a shows a SEM image of the mechanochemically prepared composite A (Al-3.93wt% Bi-3.93wt% In-5.24wt% Sn). Fig. 3b, c, d and e depicts the corresponding EDS elemental map for Al, Bi, In and Sn, respectively. Red represents Al atoms; purple, orange and green represent Bi, In and Sn, respectively.



**Figure 2.** SEM micrographs of composites (a) Al-InBi, (b) Al-InSn<sub>4</sub>, (c) Al-In<sub>3</sub>Sn and (d) quaternary Composite A (Al-3.93 wt% Bi-3.93 wt% In- 5.24 wt% Sn), showing cold welding of smaller Al particles onto each other and onto larger particles.

Fig. 3 clearly shows that the activation compounds (Bi, In and Sn) were equally distributed on the Al surface and did not aggregate at certain points. Furthermore, the complete distribution of Sn and Bi on the Al surface is important for the composite combinations of Al-Sn and Al-Bi. Both these combinations offer easy electron transfer from Al (anode) to Sn and Bi (cathodes) in the microgalvanic cell when the hydrolysis reaction of Al and water occurs [13,52,53]. Bi and Sn has a positive effect on Al hydrolysis, as an Al-Bi/Sn composites has an open circuit potential of -1.85 V, which is lower than the -1.77 V of pure Al [36]. Though, Sn does not form intermetallic phases with Al [54], the presence of Sn in Al-Sn composites has indicated an increase in the thermodynamic activity of Al [55]. Al-In composites displayed limited reactivity during hydrolysis with pure water at room temperature [56]. Additionally, it is highly likely that intermetallic phases (InBi, In<sub>3</sub>Sn, and InSn<sub>4</sub>) would occur on the surface of Al particles.



**Figure 3.** (a) SEM micrographs of quaternary composite A (Al-3.93 wt% Bi-3.93 wt% In-5.24 wt% Sn), and the corresponding EDS mapping for (b) Al, (c) Bi, (d) In and (e) Sn.

### 3.3. Characterization and hydrolysis kinetics of ternary Al-In-Bi and Al-In-Sn composites

XRD analysis of Al-In-Bi and Al-In-Sn was performed to investigate the intermetallic phases present in the ternary composites. Three prominent intermetallic phases formed during the mechanochemical preparation of Al composites: InBi, In<sub>3</sub>Sn and InSn<sub>4</sub>. They are believed to be

responsible for the activation of Al and/or partake in the work hardening of Al particles, which induces structural failure of Al particles.

Fig. 4 shows XRD patterns of the Al composites Al-InSn<sub>4</sub>, Al-InBi and Al-In<sub>3</sub>Sn. The wt% values of these composites are presented in Table 1. The wt% value of each of the composites coincided with the mole ratio of their corresponding intermetallic phases. Composites Al-InSn<sub>4</sub> and Al-In<sub>3</sub>Sn had In:Sn mole ratios of 1:4 and 3:1, respectively, while composite Al-InBi had a In:Bi mole ratio of 1:1. In each case, intermetallic phases formed according to the predesignated mole ratios. Composites Al-InSn<sub>4</sub> and Al-In<sub>3</sub>Sn only formed InSn<sub>4</sub> and In<sub>3</sub>Sn, respectively. It was expected that some competition should exist between the formation of the two intermetallic phases; however, no competition was observed, and InSn<sub>4</sub> and In<sub>3</sub>Sn were selectively synthesized. In the case of composite Al-InBi, InBi formed exclusively. No intermetallic Al-In and Al-Bi phases were detected. This may be ascribed to the low solubility of In and Bi in the Al matrix [57,58].

A study by Wang et al. (2012) indicated the presence of In<sub>3</sub>Sn and InSn<sub>4</sub> (determined by XRD) in Al-Ga-In-Sn-Fe composites prepared by an arc melting method. Some composites had close to 100% yields, when hydrolyzed in hot (50 °C) water [59]. However, an objective of this study included to selectively synthesize In-Bi and In-Sn intermetallic phases on the surface of Al particles, using a mechanochemical preparation method. Additionally, the study by Wang et al. (2012) included Ga, which could be completely excluded from composites prepared in this study.

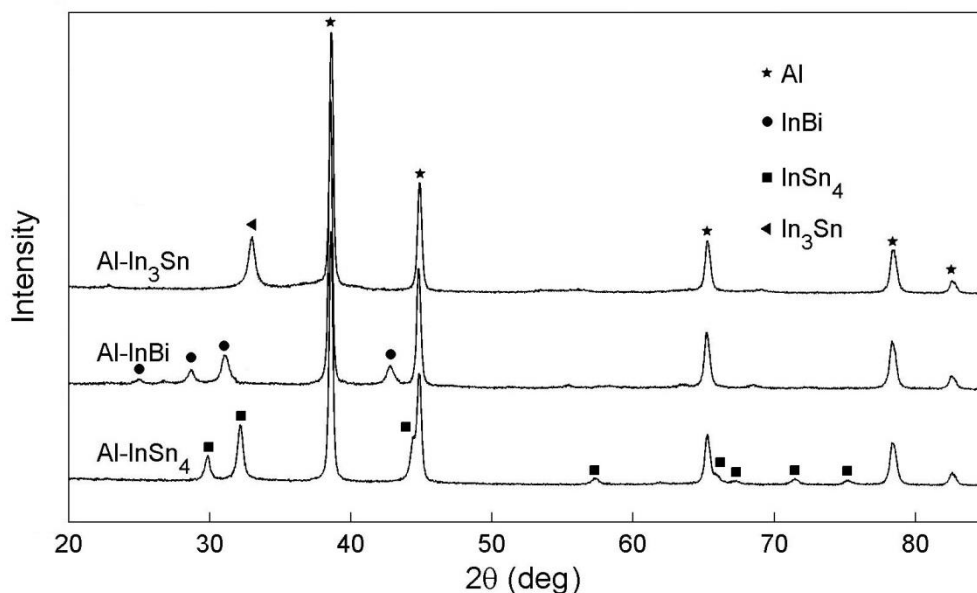


**Figure 4.** XRD patterns of ternary composites Al-InSn<sub>4</sub>, Al-InBi and Al-In<sub>3</sub>Sn. Experimental conditions used for ball milling of composites: 3 h, 450 rpm, nitrogen atmosphere. Amounts (wt%) of activation compounds (Bi, In and Sn) varied, in the range 2.54–10.55 wt%. Al was kept at 86.91 wt%.

The selectively synthesized intermetallic phase containing composites were hydrolyzed to investigate the respective effects of InSn<sub>4</sub>, InBi and In<sub>3</sub>Sn during Al hydrolysis. Fig. 5 shows the

hydrogen generation rates of the Al composites Al-InSn<sub>4</sub>, Al-InBi and Al-In<sub>3</sub>Sn under ambient conditions.

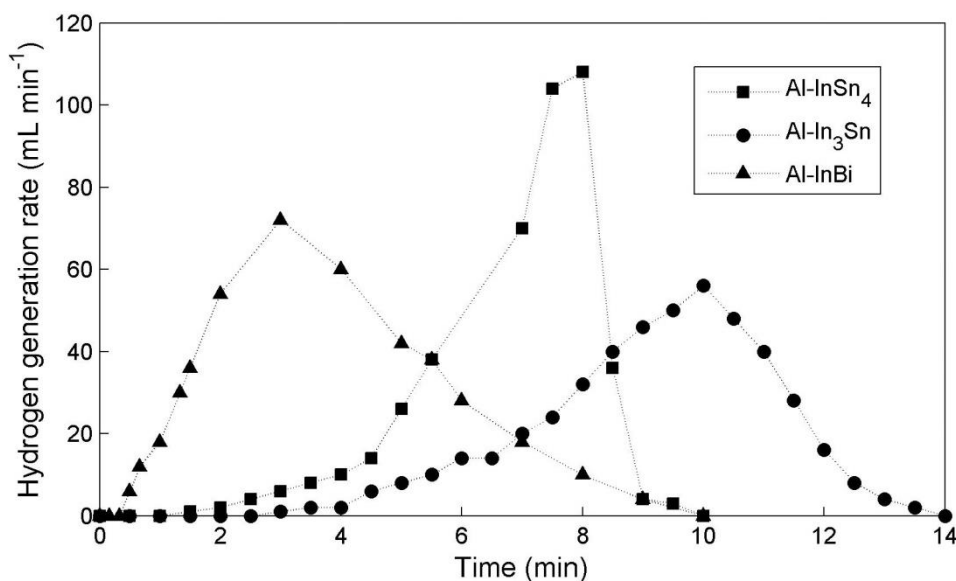


**Figure 5.** Hydrogen generation rates of ternary composites Al-InSn<sub>4</sub>, Al-InBi and Al-In<sub>3</sub>Sn. Hydrolysis parameters were kept constant: 10 mL tap water as hydrolysis solution, standard temperature and pressure.

Fig. 5 shows that Al-InBi reached its peak hydrogen generation rate of approximately 76 mL min<sup>-1</sup> after 3 min of coming into contact with water. The average hydrogen generation rate (for 0.2 g Al composite) was 24 mL min<sup>-1</sup>. Al-InSn<sub>4</sub> peaked at 120 mL min<sup>-1</sup> after 8 min and rapidly decreased thereafter. Al-In<sub>3</sub>Sn had a generation rate of 56 mL min<sup>-1</sup> after 10 min. Al-InSn<sub>4</sub> and Al-In<sub>3</sub>Sn had average hydrogen generation rates of 22 and 15 mL min<sup>-1</sup>, respectively. It is evident that each intermetallic phase present in the composites (InBi, InSn<sub>4</sub> and In<sub>3</sub>Sn) had unique hydrolysis kinetics.

The different induction times, i.e., delay before the initiation of hydrolysis, of each Al composite, due to the presence of different intermetallic phases, can be utilized to control the rate of hydrogen release. Al-InBi had the fastest hydrogen generation rate and an approximate hydrogen yield of 95%, whereas Al-In<sub>3</sub>Sn and Al-InSn<sub>4</sub> had slower hydrogen generation rates and approximate hydrogen yields of 93%. Al-InBi had an induction time of 20 s before hydrolysis was initiated, whereas the induction times of Al-InSn<sub>4</sub> and Al-In<sub>3</sub>Sn were 60 and 150 s, respectively. The composites thus had different induction times and different reaction kinetics. Al-InSn<sub>4</sub> had a peak hydrogen generation rate of 108 mL min<sup>-1</sup> after 8 min of coming into contact with water, but reactivity rapidly decreased after reaching this peak. Al-InBi reached a peak hydrogen generation rate 72 mL min<sup>-1</sup> after 3 min, whereafter the reactivity steadily decreased. Al-In<sub>3</sub>Sn had a peak generation rate of 56 mL min<sup>-1</sup> after 10 min. It had the slowest reaction kinetics and it displayed similar reaction kinetics to Al-InSn<sub>4</sub>.

It was observed that the composite Al-InBi generated particles with high reactivity surfaces, whereas composites Al-InSn<sub>4</sub> and Al-In<sub>3</sub>Sn generated particles with a protective layer on the surface of

the particles. It is possible that during hydrolysis, water had to diffuse through the coinciding intermetallic phases, i.e.,  $\text{InSn}_4$  and  $\text{In}_3\text{Sn}$ , before hydrolysis of the underlying Al could commence. Water diffused through  $\text{InSn}_4$  faster than through  $\text{In}_3\text{Sn}$ , as indicated by the different induction times of the two composites Al- $\text{InSn}_4$  and Al- $\text{In}_3\text{Sn}$ . Another possible reaction mechanism may be ascribed to micro-galvanic activity between Al-Sn, and that Al- $\text{InSn}_4$  had a shorter induction period due to an increased Sn content compared to the slower reacting Al- $\text{In}_3\text{Sn}$  composite. Al- $\text{InBi}$  reacted with water upon contact, which is indicative of a chemically reactive surface. It is likely that the short induction time may be ascribed to the high micro-galvanic activity of Al-Bi, resulting in the almost instantaneous hydrolysis of Al.

### 3.4. Formation kinetics of intermetallic phases during quaternary composite preparation

During ternary Al composite hydrolysis, the hydrogen yield (%) of the investigated composites was relatively constant, but the quaternary composites displayed some differences in terms of hydrolysis kinetics. Hydrolysis parameters were kept constant throughout, meaning that the only possible reason for variations in hydrolysis kinetics was the presence of different intermetallic phases and/or the amounts thereof.

Fig. 6 shows the XRD patterns of composites A, B, C and D. Ball milling parameters were kept constant. Composites B, C and D had different amounts of the activation compounds Bi, In and Sn: 2.62, 3.93 and 6.54 wt%.

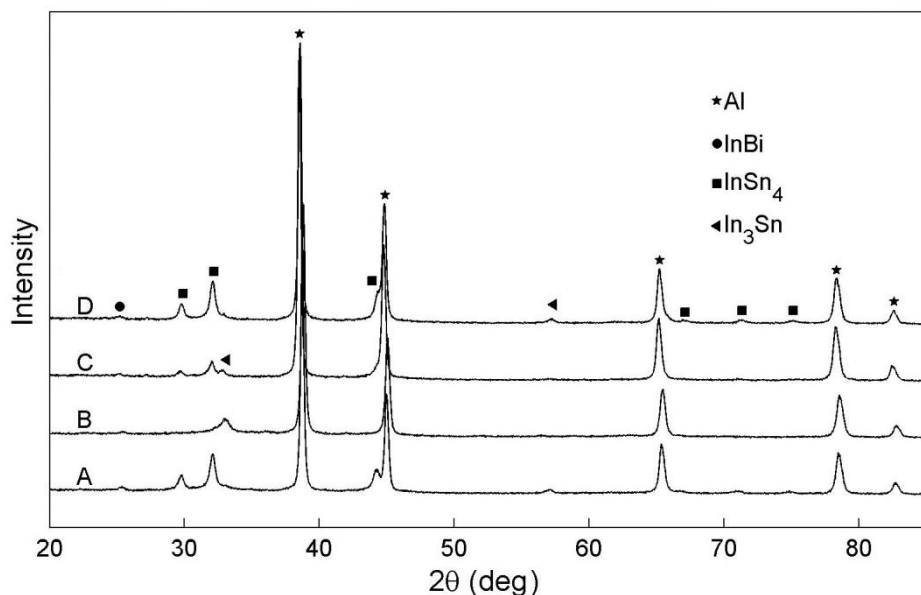


**Figure 6.** XRD patterns of quaternary Al composites A (Al-3.93 wt% Bi-3.93 wt% In-5.24 wt% Sn), B (Al-6.54 wt% Bi-3.93 wt% In-2.62 wt% Sn), C (Al-3.93 wt% Bi-6.54 wt% In-2.62 wt% Sn) and D (Al-3.93 wt% Bi-2.62 wt% In-6.54 wt% Sn). Experimental conditions used for ball milling of composites: 3 h, 450 rpm, nitrogen atmosphere. Amounts (wt%) of activation compounds (Bi, In and Sn) varied, in the range 2.62–6.54 wt%. Al was kept at 86.91 wt%.

It is evident from Fig. 6 that InBi, In<sub>3</sub>Sn and InSn<sub>4</sub> formed during ball milling of the quaternary composites. Composite B had the largest fraction of Bi present (6.54 wt%). Only InBi and In<sub>3</sub>Sn were observed. It was accepted that, on an atomic scale, the formation of InBi consumed the majority of the In and Bi atoms, followed by In<sub>3</sub>Sn consuming the remainder of the In atoms.

InBi, In<sub>3</sub>Sn and InSn<sub>4</sub> intermetallic phases were present in composite C. Bi atoms were consumed to form InBi, whereas the remainder of the In and Sn atoms competed to form In<sub>3</sub>Sn and InSn<sub>4</sub>. In the case of composite D, prominent peaks of all three intermetallic phases were observed. A possible reason for the three prominent peaks is that an increase in the number of Sn atoms could easily consume the In atoms to form In<sub>3</sub>Sn and InSn<sub>4</sub>. Composites A and D had similar XRD patterns. The small wt% increase in In and decrease in wt% Sn resulted in the peak drift observed at the 2 $\theta$  position 44. This is due to the more complete formation of In<sub>3</sub>Sn, which can be explained by an increase in In atoms that are readily available to composite with Sn atoms.

It also emerged from Fig. 6 that InBi had slightly faster formation kinetics than In<sub>3</sub>Sn and InSn<sub>4</sub>. The formation kinetics of In<sub>3</sub>Sn and InSn<sub>4</sub> depended on the availability of both In and Sn atoms and the absence of Bi atoms. In Fig. 4, where Bi atoms were not present during ball milling, no competition was observed between In<sub>3</sub>Sn and InSn<sub>4</sub> due to the atomic ratios of In:Sn; a 3:1 In:Sn ratio led to the formation of In<sub>3</sub>Sn while a 1:4 In:Sn ratio led to the formation of InSn<sub>4</sub>. Fig. 6 displays clear evidence of competitive formation between In<sub>3</sub>Sn and InSn<sub>4</sub>, which, to a certain extent, can be controlled by manipulating the mole ratios of In:Sn.

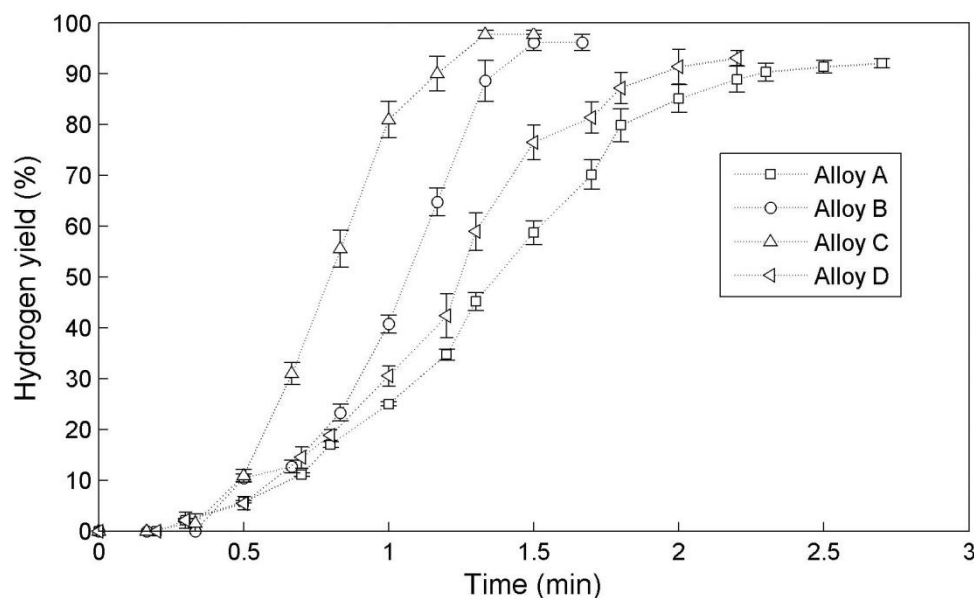


**Figure 7.** Average hydrogen yield (%) of quaternary Al composites A (Al-3.93 wt% Bi-3.93 wt% In-5.24 wt% Sn), B (Al-6.54 wt% Bi-3.93 wt% In-2.62 wt% Sn), C (Al-3.93 wt% Bi-6.54 wt% In-2.62 wt% Sn) and D (Al-3.93 wt% Bi-2.62 wt% In-6.54 wt% Sn). Experimental conditions used for ball milling of composites: 3 h, 450 rpm, nitrogen atmosphere. Amounts (wt%) of activation compounds (Bi, In and Sn) varied, in the range 2.62–6.54 wt%. Al was kept at 86.91 wt%.

Fig. 7 presents the average hydrogen yield (%) of quaternary Al composites A, B, C and D, respectively. In most cases, reactivity of quaternary Al composites did not differ substantially. Reported reactivities had approximate hydrogen yields of 91.2–98%. Induction times were relatively short and ranged from 20 to 30 s. The hydrolysis reactions were completed within 90 s (fastest) and 170 s (slowest) after coming into contact with water.

Results of the hydrolysis of quaternary Al composites were compared with results of the hydrolysis of the ternary Al composites. It is clearly evident that combinations of intermetallic phases displayed a synergetic effect with regard to reaction kinetics. The ternary composite Al-InBi had the shortest induction time (Fig. 5). This resulted in InBi containing quaternary composites displaying reduced induction periods, due to the *in situ* generated heat being released by the fast reacting InBi containing Al particles. The released heat catalyzed the slower reacting InSn<sub>4</sub> and In<sub>3</sub>Sn containing Al particles. As far as the authors could assess, no literature is available in the peer-reviewed public domain on hydrogen generation of Al-In-Bi-Sn composites (excluding Ga) prepared through a mechanochemical activation method. Though, a study by Huang et al. (2015) prepared high hydrogen yielding Al-Ga-In<sub>3</sub>Sn and Al-Ga-InBi composites, as well as a relatively low hydrogen yielding Al-Ga-InSn<sub>4</sub> composites, prepared through a melting method [60].

### 3.5. Proposed formation mechanism with regards to intermetallic phase formation

The authors propose the following two mechanisms that could play a role in intermetallic formation of InBi, In<sub>3</sub>Sn and InSn<sub>4</sub>. (1) During ball milling of ternary composites containing Al-Bi-In or Al-In-Sn, the atomic ratio will determine which intermetallic phases will form. For instance, if a 1:4 In:Sn atomic ratio is present, InSn<sub>4</sub> will form exclusively. A possible explanation for this is that, during ball milling, there will be a greater chance that a predetermined ratio of atoms will be caught between composite-forming milling-ball collisions. The same can be accepted for a 3:1 In:Sn atomic ratio. In the case of Al-Bi-In, InBi will form until either In and/or Bi is consumed. (2) During quaternary composite Al-In-Bi-Sn preparation, the formation of all three intermetallic phases (InBi, In<sub>3</sub>Sn and InSn<sub>4</sub>) may be present. In this study, small InBi peaks were observed in all Al composites containing Bi as a starting material. The presence of Bi induces a degree of competitive formation between In and Sn containing intermetallic phases, i.e., In<sub>3</sub>Sn and InSn<sub>4</sub>. Thus, the second mechanism for quaternary composite ball milling can be summarized as the formation of either InBi, In<sub>3</sub>Sn and/or InSn<sub>4</sub>, which is tantamount to the coincidental presence of atoms during collisions of milling balls and can be controlled by manipulating the quantity (wt%) of each of the activation compounds added.

### 3.6. Effects of mass ratio ( $m_{Al\ powder}/m_{water}$ ) and temperature on the hydrolysis reaction

Al-InSn<sub>4</sub> was chosen to depict the effects of mass ratio and temperature as it represents a ternary composite with a reactivity between the fast reacting Al-InBi and slower reacting Al-In<sub>3</sub>Sn. Here, a mass ratio of 1:20 is defined as 1 g of Al powder reacting with 20 mL of water. All mass ratios

were derived similarly. Fig. 8 depicts the effect of different mass ratios on (a) hydrogen yield and (b) reaction temperature. The mass ratio ranged from 1:20 to 1:500.

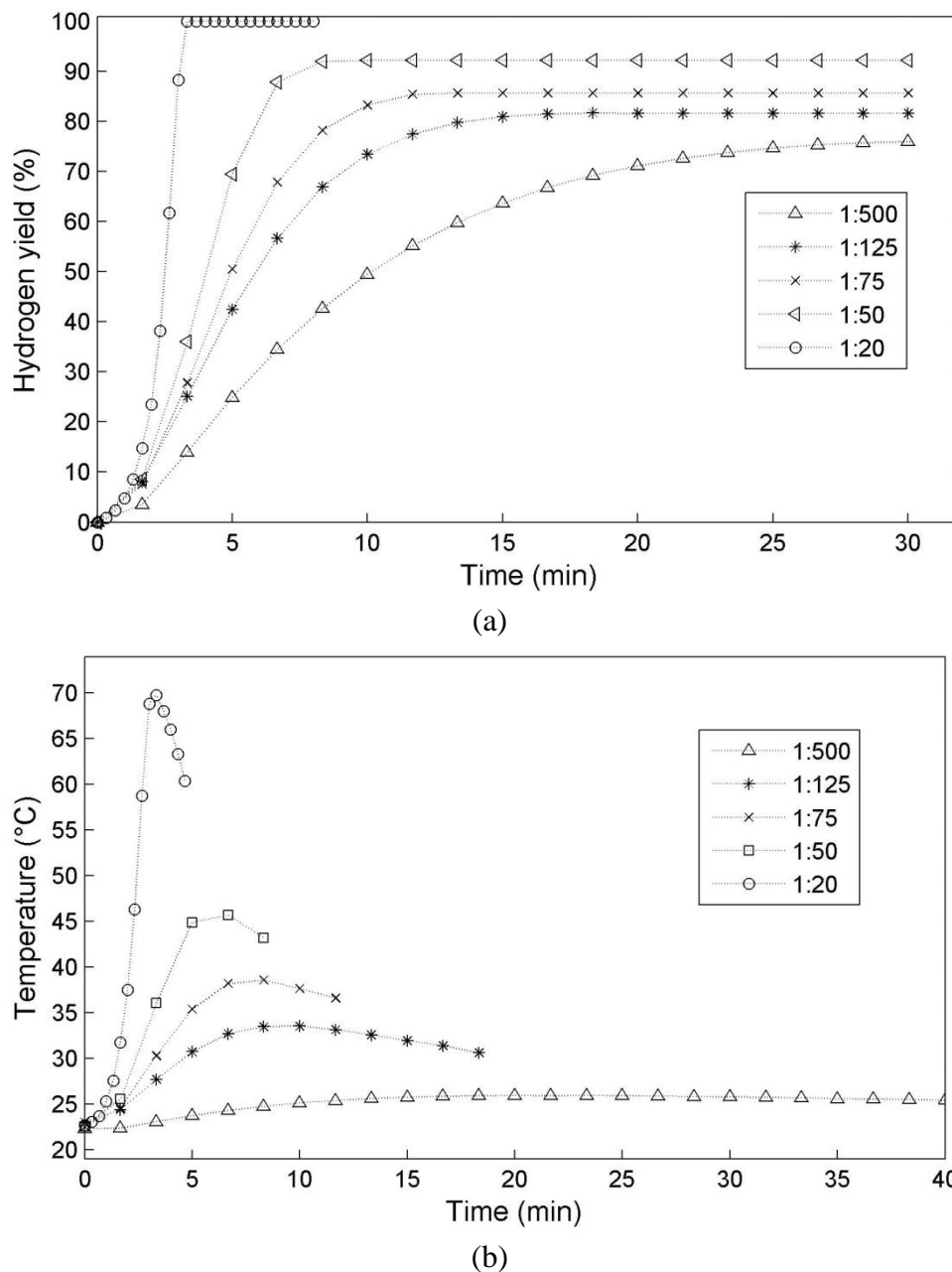


**Figure 8.** Effect of different mass ratios ( $m_{Al-InSn_4}/m_{water}$ ) on (a) hydrolysis kinetics of Al-InSn<sub>4</sub> and (b) change in reaction temperature during the hydrolysis reaction.

Results presented in Fig. 8a indicate an increase in the hydrolysis reaction rate and hydrogen yield as the mass ratio  $m_{Al-InSn_4}/m_{water}$  decreased from 1:500 to 1:20. The hydrogen yield for the 1:20 mass ratio hydrolysis reaction was 100% and it decreased to 76.2% as the mass ratio was increased to 1:500. The Al hydrolysis reaction is dependent on reaction temperature [13,61]. Thus, the decrease in hydrogen yield was caused by the decrease in reaction temperature. Fig. 8b depicts the effect that water volume has on the change in reaction temperature during hydrolysis reactions of ternary Al composite Al-InSn<sub>4</sub>. The reaction temperature of the 1:20 mass ratio hydrolysis reactions increased by

$48.0 \pm 2.8$  °C, whereas a  $5.6 \pm 0.8$  °C increase was observed during the 1:500 hydrolysis reactions. During the hydrolysis reaction, heat ( $\Delta H = -444.4$  kJ mol<sup>-1</sup>) [42] is released and, in turn, catalyzes the hydrolysis reaction. An increase in water volume decreased the reaction temperature during hydrolysis as the *in situ* generated heat mitigates away from the immediate reaction sites (Al particles undergoing hydrolysis). This resulted in a slower hydrogen generation rate and a decrease in hydrogen yield. As expected, a similar trend was observed for all Al composites investigated in this study.

If the Al composites prepared in this study were to be considered for PEMFC applications, hydrogen has to be generated at a relatively steady rate, due to the fact that PEMFCs require a steady supply of hydrogen gas to operate optimally. Thus, the Al hydrolysis reaction has to be manipulated in such a way to ensure a controllable rate of hydrogen generation. It is clear from Figure 8 that larger hydrolysis mass ratios resulted in a decrease in reaction temperature, which in turn reduces the hydrogen generation rate (and hydrogen yields). For example, Al-InSn<sub>4</sub> hydrolysis performed at a 1:20 mass ratio had a 100% hydrogen yield, a reaction temperature increase of 48 °C, and a peak hydrogen generation rate of approximately 280 mL min<sup>-1</sup>. Such reaction temperatures and hydrogen flow rates may cause complications during PEMFC applications. However, the same hydrolysis reaction performed at a 1:500 mass ratio will result in a reaction temperature increase of 5.6 °C, and a peak hydrogen generation rate of 18 mL min<sup>-1</sup>. Thus, it is indicative that a certain amount of the Al-InSn<sub>4</sub> composite may be hydrolyzed to provide a PEMFC with a steady hydrogen stream. Though, hydrolysis at such a large mass ratio, i.e. 1:500, did result in a decrease in hydrogen yield, the hydrogen generation rate would be sufficient for PEMFC application.

Energy applications (PEMFC application) using this method of hydrogen generation is still under development and requires further improvements and developments, it may be utilized by several sectors. An advantage of this method is the ability to generate hydrogen on-demand and on-site, removing the need for hydrogen storage and transport. According to the Russian Skolkovo Foundation (web reference: <https://sk.ru/news/m/wiki/14838/download.aspx>) the portable charging devices market is an estimated \$34bn market. Additionally, markets for unmanned aerial vehicles (UAVs), various military and emergency energy applications, portable low power electronic devices, and underground mining equipment are large, and the value yet to be determined. Al hydrolysis (Reactions 1 and 2) has a theoretical hydrogen mass yield of 11% based on the mass of Al. Considering the high hydrogen yields obtained from composites prepared in this study, an approximate 2.2 kWh kg<sup>-1</sup> specific electric energy may be generated through a PEMFC [62]. It is worth mentioning that electrochemical energy systems, such as hydrogen fuel cells, require hydrogen of a high purity. “Al-to-hydrogen” system described in this paper generates PEM-grade purity hydrogen. At this stage we envisage that the described technology could be used for power tools at construction sites, cell phones, laptops, professional digital video cameras, etc., in other words, niche, small-scale applications. For military applications, typical requirements would include, but not limited to, low noise level, low heat signature, lower weight, etc. and power rating not exceeding 1 kW. “Al-to-hydrogen” system could address all these requirements.

Fig. 8a and b reflects the major influence of reaction temperature on hydrogen generation. The following Arrhenius equation was used to determine this effect:

$$k = A \exp^{(-E_a/RT)} \quad (1)$$

It gives the dependence of a rate constant ( $k$ ) on temperature ( $T$ ) and activation energy ( $E_a$ ). By determining  $k$  from the maximum flow rates obtained at different temperatures (23–50 °C) and using eqn. (1), the activation energies of the ternary Al composites were calculated to be 47.2 kJ mol<sup>-1</sup> for Al-InBi, 57.5 kJ mol<sup>-1</sup> for Al-In<sub>3</sub>Sn and 62.1 kJ mol<sup>-1</sup> for Al-In<sub>3</sub>Sn from the plot of reaction rate  $k$  against the reciprocal temperature, as presented in Fig. 9. The coefficient of determination ( $R^2$ ) ranged between 0.9674 and 0.9927.

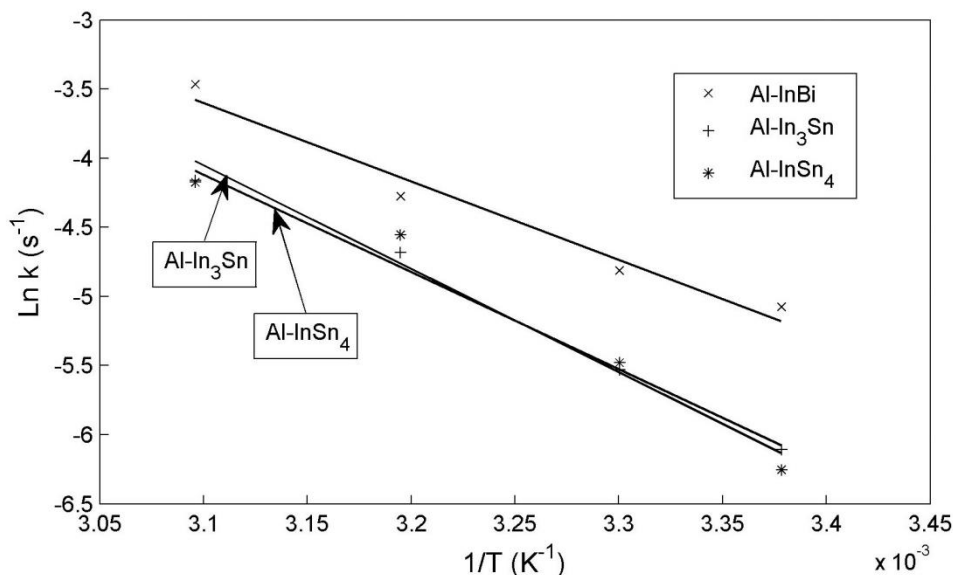


**Figure 9.** The Arrhenius plot for the maximum hydrolysis reaction rates of the reaction between ternary Al composites (Al-InBi, Al-In<sub>3</sub>Sn and Al-InSn<sub>4</sub>) and water.

The ternary Al composite activation energies coincide with the activation energies of Al activated by mechanochemical preparation methods using NaCl ( $63.1 \pm 3.1$  kJ mol<sup>-1</sup>) [63] and graphite ( $61 \pm 10$  kJ mol<sup>-1</sup>) [64]. The lower activation energy of Al-InBi, compared with Al-InSn<sub>4</sub> and Al-In<sub>3</sub>Sn, corresponds with the induction times of all three ternary composites, e.g., Al-InBi had the lowest activation energy and the shortest induction time, whereas Al-InSn<sub>4</sub> had the highest activation energy and the longest induction time.

### 3.7. Analysis of hydrolysis residues

The hydrolysis residues of ternary Al composites and of Composite A, hydrolyzed at different water volumes, were characterized by XRD. Results are presented in Fig. 10a and b, respectively. XRD spectra of hydrolyzed residues were more detailed than spectra of unhydrolyzed Al composites (Figs 4 and 6) due to the absence of large, overshadowing Al peaks.

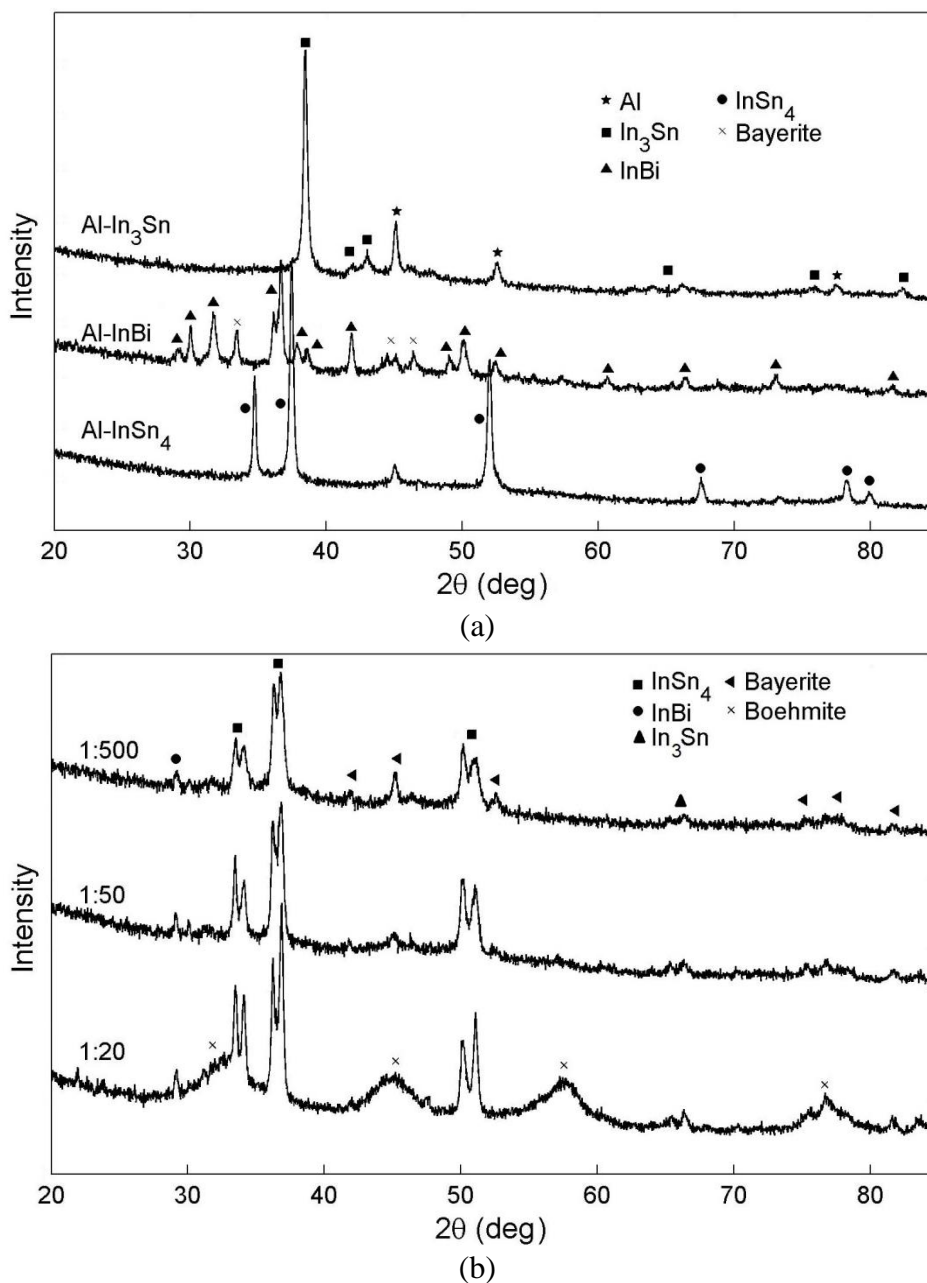


**Figure 10.** Hydrolysis residues of (a) ternary Al composites and (b) quaternary Composite A at various  $m_{Al\ powder}/m_{water}$  ratios.

It is evident from Fig. 10a and b that the residues mainly consisted of two Al hydroxide phases (bayerite and boehmite), each of the composites coinciding intermetallic phases (InBi, In<sub>3</sub>Sn and/or InSn<sub>4</sub>), and some unreacted Al peaks. Fig. 10a shows many small bayerite peaks (some too small to indicate) and the intermetallic phases present. Small Al peaks indicate that some of the Al did not undergo hydrolysis. The presence of the intermetallic phases indicates that they did not react with water; hence, the total volume of hydrogen originated from the hydrolysis of Al.

It is evident from Fig. 10b that a decrease in water volume led to a decrease in bayerite peak intensity and an increase in boehmite peak intensity. This is due to the large increase in temperature as

the  $m_{\text{Al power}}/m_{\text{water}}$  increased. At low temperatures, Al hydrolyzes to form bayerite. At higher temperatures, the bayerite decomposes to form boehmite. Both of these Al hydroxide phases are considered to be environmentally benign. This observation is in agreement with observations made by Huang et al. [60] and du Preez and Bessarabov (2017) [45].

#### 4. CONCLUSIONS

A mechanochemical activation method was used to prepare various Al composites containing Bi, In and Sn as activation compounds. The hydrogen generation of activated Al upon reacting with tap water was investigated under standard temperature and pressure conditions. It was concluded that the hydrogen generation of ball-milled Al depended on the activation compounds, *in situ* generated intermetallic phases of the activation compounds and the amounts of *in situ* generated intermetallic phases.

Experimental results of this study can be summarized as follows:

(1) High yield ternary composites were successfully prepared, without the use of Ga. The intermetallic phases responsible for the activation of Al were successfully synthesized, identified and characterized. InBi containing composites had the shortest induction time and slightly higher hydrogen yields than the InSn<sub>4</sub> and In<sub>3</sub>Sn containing composites. InBi containing composites had the fastest reaction time, followed by the InSn<sub>4</sub> and In<sub>3</sub>Sn containing composites.

(2) Highly reactive quaternary composites were successfully prepared. Characterization revealed that all prepared quaternary composites contained InBi, and InSn<sub>4</sub> and/or In<sub>3</sub>Sn, depending on the amount of activation compounds added. Hydrolysis reactions were relatively fast due to the presence of InBi. The heat released from InBi containing Al particles catalyzed the slower reacting InSn<sub>4</sub> and In<sub>3</sub>Sn containing Al particles.

(3) The activation energies of ternary composites were determined to be between 47.2 and 62.1 kJ mol<sup>-1</sup>. Al-InBi had the lowest activation energy, which suggests it follows a different reaction path to Al-InSn<sub>4</sub> and Al-In<sub>3</sub>Sn.

(4) The hydrolysis reactions had a relatively large dependence on reaction temperature. Increased reaction temperatures expedited reaction rates and hydrogen yields. Thus, the hydrogen generation rate could be altered by controlling the reaction temperature, possibly at the expense of the hydrogen yield.

(5) XRD analysis of hydrolysis residues indicated that the intermetallic phases present in each of the composites did not hydrolyze, hence the total hydrogen content originated from the hydrolysis of Al. Low temperature hydrolysis produced boehmite whereas higher temperatures induced decomposition of boehmite to bayerite. Boehmite and bayerite are considered to be environmentally benign.

#### ACKNOWLEDGMENTS

Department of Science and Technology (DST) HySA Infrastructure Center of Competence at the North West University, South Africa, is acknowledged for financial support.

**References**

1. C. C. Elam, C. E. G. Padró, G. Sandrock, A. Luzzi, P. Lindblad and E. F. Hagen, *Int. J. Hydrogen Energ.*, 28 (2003) 601.
2. Y. Liu, X. Wang, Z. Dong, H. Liu, S. Li, H. Ge and M. Yan, *Energy*, 53 (2013) 147.
3. J. Macanás, L. Soler, A. M. Candela, M. Muñoz and J. Casado, *Energy*, 36 (2011) 2493.
4. H. Z. Wang, D. Y. C. Leung, M. K. H. Leung and M. Ni, *Renew. Sust. Energ. Rev.*, 13 (2009) 845.
5. Y. J. Chai, Y. M. Dong, H. X. Meng, Y. Y. Jia, J. Shen, Y. M. Huang and N. Wang, *Energy*, 68 (2014) 204.
6. M. Balat, *Int. J. Hydrogen Energ.*, 33 (2008) 4013.
7. M. Ball and M. Wietschel, *Int. J. Hydrogen Energ.*, 34 (2009) 615.
8. P. V. Gosavi and R. B. Biniwale, *J. Power Sources*, 222 (2013) 1.
9. J. A. Turner, *Science*, 305 (2004) 972.
10. X. Chen, Z. Zhao, M. Hao and D. Wang, *J. Power Sources*, 222 (2013) 188.
11. D. Bessarabov, G. Human, A. J. Kruger, S. Chiuta, P. M. Modisha, S. P. du Preez, S. P. Oelofse, I. Vincent, J. Van Der Merwe, H. W. Langmi, J. Ren and N. M. Musyoka, *Int. J. Hydrogen Energ.*, 42 (2017) 13568.
12. A. J. Esswein and D. G. Nocera, *Chem. Rev.*, 107 (2007) 4022.
13. A. V. Ilyukhina, A. S. Ilyukhin and E. I. Shkolnikov, *Int. J. Hydrogen Energ.*, 37 (2012) 16382.
14. B. Sakintuna, F. Lamari-Darkrim and M. Hirscher, *Int. J. Hydrogen Energ.*, 32 (2007) 1121.
15. B. C. Steele and A. Heinzl, *Nature*, 414 (2001) 345.
16. S. Elitzur, V. Rosenband and A. Gany, *Int. J. Hydrogen Energ.*, 42 (2017) 14003.
17. K. Wegner, H. C. Ly, R. J. Weiss, S. E. Pratsinis and A. Steinfeld, *Int. J. Hydrogen Energ.*, 31 (2006) 55.
18. M.-H. Grosjean, M. Zidoune, L. Roué and J.-Y. Huot, *Int. J. Hydrogen Energ.*, 31 (2006) 109.
19. M.-H. Grosjean and L. Roué, *J. Alloy Compd.*, 416 (2006) 296.
20. K. Mahmoodi and B. Alinejad, *Int. J. Hydrogen Energ.*, 35 (2010) 5227.
21. E. Tzimas, C. Filiou, S. D. Petevs and J. Veyret, Hydrogen storage: state-of-the-art and future perspective, Institute of Energy, Petten, The Netherlands, 2003.
22. O. V. Kravchenko, K. N. Semenenko, B. M. Bulychev and K. B. Kalmykov, *J. Alloy Compd.*, 397 (2005) 58.
23. A. V. Parmuzina and O. V. Kravchenko, *Int. J. Hydrogen Energ.*, 33 (2008) 3073.
24. E. David and J. Kopac, *J. Hazard. Mater.*, 209–210 (2012) 501.
25. B. Alinejad and K. Mahmoodi, *Int. J. Hydrogen Energ.*, 34 (2009) 7934.
26. H. Zou, S. Chen, Z. Zhao and W. Lin, *J. Alloy Compd.*, 578 (2013) 380.
27. X. Huang, T. Gao, X. Pan, D. Wei, C. Lv, L. Qin and Y. Huang, *J. Power Sources*, 229 (2013) 133.
28. H. Teng, T. Lee, Y. Chen, H. Wang and G. Cao, *J. Power Sources*, 219 (2012) 16.
29. M. Baniamerian and S. Moradi, *J. Alloy Compd.*, 509 (2011) 6307.
30. D. Belitskus, *J. Electrochem. Soc.*, 117 (1970) 1097.
31. L. Soler, J. Macanás, M. Muñoz and J. Casado, *Int. J. Hydrogen Energ.*, 32 (2007) 4702.
32. S. S. Martinez, L. Albañil Sánchez, A. A. Álvarez Gallegos and P. Sebastian, *Int. J. Hydrogen Energ.*, 32 (2007) 3159.
33. E.-D. Wang, P.-F. Shi, C.-Y. Du and X.-R. Wang, *J. Power Sources*, 181 (2008) 144.
34. X. Huang, C. Lv, Y. Huang, S. Liu, C. Wang and D. Chen, *Int. J. Hydrogen Energ.*, 36 (2011) 15119.
35. J. T. Ziebarth, J. M. Woodall, R. A. Kramer and G. Choi, *Int. J. Hydrogen Energ.*, 36 (2011) 5271.
36. M. Q. Fan, F. Xu and L. X. Sun, *Int. J. Hydrogen Energ.*, 32 (2007) 2809.

37. S. Liu, M.-Q. Fan, C. Wang, Y.-X. Huang, D. Chen, L.-Q. Bai and K.-Y. Shu, *Int. J. Hydrogen Energ.*, 37 (2012) 1014.
38. A. N. Streletskii, I. V. Kolbanev, A. B. Borunova and P. Y. Butyagin, *J. Mater. Sci.*, 39 (2004) 5175.
39. H.-W. Wang, H.-W. Chung, H.-T. Teng and G. Cao, *Int. J. Hydrogen Energ.*, 36 (2011) 15136.
40. P. Dupiano, D. Stamatis and E. L. Dreizin, *Int. J. Hydrogen Energ.*, 36 (2011) 4781.
41. J. L. López-Miranda and G. Rosas, *Int. J. Hydrogen Energ.*, 41 (2016) 4054.
42. M. Q. Fan, L. X. Sun, F. Xu, D. Mei, D. Chen, W. X. Chai, F. L. Huang and Q. M. Zhang, *Int. J. Hydrogen Energ.*, 36 (2011) 9791.
43. A. Ilyukhina, O. Kravchenko, B. Bulychev and E. Shkolnikov, *Int. J. Hydrogen Energ.*, 35 (2010) 1905.
44. H. Wang, Y. Chang, S. Dong, Z. Lei, Q. Zhu, P. Luo and Z. Xie, *Int. J. Hydrogen Energ.*, 38 (2013) 1236.
45. S. P. du Preez and D. G. Bessarabov, *Int. J. Hydrogen Energ.*, (2017) <http://dx.doi.org/10.1016/j.ijhydene.2017.05.211>
46. Z. Zhao, X. Chen and M. Hao, *Energy*, 36 (2011) 2782.
47. E. Czech and T. Troczynski, *Int. J. Hydrogen Energ.*, 35 (2010) 1029.
48. S. S. Razavi-Tousi and J. A. Szpunar, *Metall. Mater. Trans. E.*, 1 (2014) 247.
49. C. Suryanarayana, *Prog. Mater. Sci.*, 46 (2001) 1.
50. S. S. Razavi-Tousi and J. A. Szpunar, *Int. J. Hydrogen Energ.*, 38 (2013) 795.
51. J. Benjamin, *Sci. Am.*, 234 (1976) 40.
52. M. Q. Fan, L. X. Sun and F. Xu, *Renew. Energy*, 36 (2011) 519.
53. M. Q. Fan, F. Xu, L.-X. Sun, J.-N. Zhao, T. Jiang and W.-X. Li, *J. Alloy Compd.*, 460 (2008) 125.
54. R. Parsons, *Handbook of electrochemical constants*, Butterworths Scientific Publications, (1959) Preston, London.
55. N. Y. Taranets, V. Nizhenko, V. Poluyanskaya and Y. V. Naidich, *Acta Mater.*, 50 (2002) 5147.
56. M.-Q. Fan, L.-X. Sun and F. Xu, *Energy Convers. and Manage.*, 51 (2010) 594.
57. F.-Q. Wang, H.-H. Wang, J. Wang, J. Lu, P. Luo, Y. Chang, X.-G. Ma and S.-J. Dong, *Trans. Nonferrous Met. Soc. China*, 26 (2016) 152.
58. V. Bhattacharya and K. Chattopadhyay, *Mater. Sci. Eng. A*, 375 (2004) 932.
59. W. Wang, W. Chen, X. M. Zhao, D. M. Chen and K. Yang, *Int. J. Hydrogen Energ.*, 37 (2012) 18672.
60. T. Huang, Q. Gao, D. Liu, S. Xu, C. Guo, J. Zou and C. Wei, *Int. J. Hydrogen Energ.*, 40 (2015) 2354.
61. J. Skrovan, A. Alfantazi and T. Troczynski, *J. Appl. Electrochem.*, 39 (2009) 1695.
62. S. Elitzur, V. Rosenband and A. Gany, *Int. J. Appl. Sci. Technol.*, 5 (2015) 112.
63. A. K. Narayana Swamy and E. Shafirovich, *Combust. Flame*, 161 (2014) 322.
64. A. Streletskii, I. Kolbanev, A. Borunova and P. Y. Butyagin, *Colloid J.*, 67 (2005) 631.